Robotized cane for locomotion assistance

Pedro Bollinger
pedro.bollinger@tecnico.ulisboa.pt

Instituto Superior Técnico, Lisboa, Portugal

November 2022

Abstract

Considering the sustained increase in the elderly population throughout the world, a growing number of people require locomotion assistance. Current technology allows for the enhancement of standard walking aids in order to improve their safety, comfort and user-friendliness. This thesis proposes an adaptive control system for a robotic cane based on an existing prototype. The controller derives from the model of an inverted pendulum and is based on a LQR, assisting the user in keeping the plant in a stable position. Additionally, gain-scheduling techniques were implemented to adjust the control to the individual characteristics of the user, specifically the preferred walking speed and cane angle. Cane usage tests were carried out with subjects in need of locomotion assistance in order to assess the real-world performance of the controller. The results were decidedly favorable, with the system exhibiting smooth, responsive and intuitive behaviour, all the while successfully adapting to the user's walking attributes.

Keywords: Robotic cane, locomotion assistance, reduced mobility, inverted pendulum, adaptive control.

1. Introduction

As life expectancy continues to rise throughout the world, the elderly comprise an increasingly large portion of the population (from 5.1% of the population aged 65 or over in 1950, to 8.2% in 2015 [1]). Furthermore, as people grow older, they tend to have more difficulty walking, as a result of impaired vision, peripheral sensation, strength, reaction time and balance. To compensate for these factors, older people generally exhibit a slower gait pattern characterized by shorter steps [6]. This reduced mobility manifests in increased sedentary behaviour when compared to other age groups [3].

As such, a growing trend among academia has been the development of technology to improve the mobility of older people. A considerable amount of research has been focused on the implementation of robotic technology in walkers [5]. Even though these devices provide a relatively greater level of support, they are usually too unwieldy, making them impractical for use in cramped or crowded spaces. Walking canes, on the other hand, are generally more compact and lighter than walkers, although offering less stability. Through the use of robotics, it is possible to increase the stability of the cane.

This project aims to develop an adaptive controller for a robotized cane that can assist people with reduced mobility, namely the elderly, in walking correctly and with relative ease. The hardware is based on an existing prototype by Neves et al. [8].

2. Literature Review

Standard walking canes are a widespread external mobility aid that provide users with balance and partial weight support. While they are less cumbersome than similar devices, including walkers and crutches, they tend to be less stable, especially when it comes to falls by retropulsion [5]. This problem can be mitigated with the use of robotics, allowing for automatic control of the velocity and angle of the cane, and thus improving stability. The following is a selection of studies pertaining to existing robotic canes.

Van Lam et al. [10], designed a robotic cane with a single omnidirectional wheel controlled by two DC motors. The model of the robotic cane was based on an inverted pendulum and was linearized using the Lie algebra method (LAM). A nonlinear disturbance observer was designed to estimate the user-applied force. The LAM-based controller compared positively against the LQR and was shown to be stable at a wide range of rod angles, with performance in self-standing mode less prone to vibrations.

Ady et al. [2], developed a robotic cane that adapts to the gait characteristics of the user. The control objective is to mimic the movement of the

impaired leg for which a control mechanism with two loops was conceived. The inner loop controls the shaft, ensuring that the handle is at a constant height, while the outer loop minimizes the tracking error between the angle of the impaired leg and that of the cane. This control scheme was reported to provide improved balance.

Neves et al. [8], developed a lightweight and compact prototype of a robotic cane which forms the basis for this thesis. The controller design was based on the unicycle model, and employed full-state feedback control. The results from real-world tests were positive, with the cane exhibiting intuitive and smooth behaviour.

3. Model

The mathematical model of the cane is based on the robotic cane prototype developed by Neves et al. [8] (pictured in figure 1) and consists of a rod and a wheel attached to the lower extremity of the rod. The DC motor that actuates the wheel is housed inside a parallelepiped, while the controller is housed in an adjacent parallelepiped. Therefore, the rod is composed of two geometrically different sections: the top section consists of a slender cylinder and the bottom section consists of the two parallelepipeds. To simplify, the two parallelepipeds are approximated as a single parallelepiped of dimensions $l_p \times d_p \times w_p$.

Figure 1: Robotic cane prototype.

A simplified schematic is shown in figure 2, where the forces and torques applied to the rod are marked in red and those applied to the wheel are marked in blue. Some of the plant's characteristics are presented in table 1, and the variables used in the model are specified in table 2.

The application of classical mechanics to the cane yields

$$\ddot{x} = \frac{\begin{pmatrix} F_m - \frac{b}{r_w^2}\dot{x} - F_z \cos\theta \sin\theta \\ -m_r g \cos\theta \sin(\alpha+\theta) + F_x \sin^2\theta \\ +m_r l \dot{\theta}^2 \sin\theta + (m_w + m_r) g \sin\alpha \end{pmatrix}}{\frac{1}{2}m_w + m_r(1-\cos^2\theta)}, \quad (1)$$

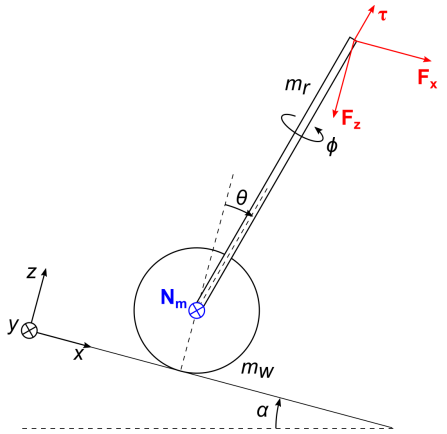

Figure 2: Schematic of the cane.

Table 1: Model parameters.

m_r	Mass of the rod	1.330 kg
m_w	Mass of the wheel	0.080 kg
r_w	Radius of the wheel	0.073 m
l	Length from axle to rod center of mass	0.147 m
b	Coefficient of friction between rod and wheel	0.25 N m s/rad
l_p	Length of the parallelepiped containing the motor	0.09 m
d_p	Depth of the parallelepiped containing the motor	0.16 m
w_p	Width of the parallelepiped containing the motor	0.075 m

Table 2: Variable terminology.

θ	Angle between the rod and the z-axis	[rad]
α	Angle between the x-axis and the horizontal plane	[rad]
ϕ	Angle around the rod axis	[rad]
x	Distance covered by the wheel	[m]
τ	Torque applied to the rod by the user	[N m]
F_m	Force applied to the wheels by the motor	[N]
F_x	x component of the force applied to the rod by the user	[N]
F_z	z component of the force applied to the rod by the user	[N]

$$\ddot{\theta} = \frac{\begin{pmatrix} (\frac{1}{2}m_w + m_r)(F_z \sin\theta + m_r g \sin(\alpha+\theta)) \\ +\frac{1}{2}m_w F_x \cos\theta - m_r(F_m - \frac{b}{r_w^2}\dot{x} \\ +(m_w + m_r) g \sin\alpha + m_r l \dot{\theta}^2 \sin\theta) \cos\theta \end{pmatrix}}{m_r l(\frac{1}{2}m_w + m_r(1-\cos^2\theta))}, \quad (2)$$

and

$$\ddot{\phi} = \frac{12\tau\cos\theta}{m_r(l_p^2 \sin^2\theta + d_p^2 \cos^2\theta + w_p^2)}. \quad (3)$$

3.1. Linearization

Although the small-angle approximation is widely used to linearize nonlinear terms, it is not suitable for the purposes of this project, as it is only accurate for $\theta \approx 0$. This limitation is undesirable, given that some cane users prefer to operate the cane at angles of up to 20°[8].

Instead, the Taylor Series linearization method was used, yielding a different linear model for each operating point. In the following equations, system variables have been rewritten as $\Delta k = k - k_0$ (for a generic variable k), where k_0 is the value of the variable at the operating point. Additionally, variables $\dot{x}$ and $\dot{\theta}$ have been re-designated as v and ω, respectively. The resulting set of linear models is expressed as

$$\dot{\mathbf{x}} = \mathbf{A}\mathbf{x} + \mathbf{B}\mathbf{u}, \tag{4}$$

$$\mathbf{y} = \mathbf{C}\mathbf{x} + \mathbf{D}\mathbf{u}, \tag{5}$$

where

$$\mathbf{x} = \begin{bmatrix}\Delta v & \Delta x & \Delta\omega & \Delta\theta & \Delta\dot{\phi} & \Delta\phi\end{bmatrix}^T; \tag{6}$$

$$\mathbf{u} = \begin{bmatrix}\Delta\alpha & \Delta F_m & \Delta F_x & \Delta F_z & \Delta\tau\end{bmatrix}^T; \tag{7}$$

$$\mathbf{A} = \begin{bmatrix} -\frac{b}{r_w^2 A(\theta_0)} & 0 & \frac{2m_r l\omega_0 \sin\theta_0}{A(\theta_0)} & \frac{K_1}{A(\theta_0)^2} & 0\ 0 \\ 1 & 0 & 0 & 0 & 0\ 0 \\ \frac{m_r b\cos\theta_0}{m_r l r_w^2 A(\theta_0)} & 0 & -\frac{2m_r^2 l\omega_0 \sin\theta_0\cos\theta_0}{m_r l A(\theta_0)} & \frac{K_2}{m_r l A(\theta_0)^2} & 0\ 0 \\ 0 & 0 & 1 & 0 & 0\ 0 \\ 0 & 0 & 0 & K_4 & 0\ 0 \\ 0 & 0 & 0 & 0 & 1\ 0 \end{bmatrix}; \tag{8}$$

$$\mathbf{B} = \begin{bmatrix} K_5 & \frac{1}{A(\theta_0)} & \frac{1-\cos^2\theta_0}{A(\theta_0)} & \frac{-\cos\theta_0\sin\theta_0}{A(\theta_0)} & 0 \\ 0 & 0 & 0 & 0 & 0 \\ K_6 & \frac{-m_r\cos\theta_0}{m_r l A(\theta_0)} & \frac{\frac{1}{2}m_w\cos\theta_0}{m_r l A(\theta_0)} & \frac{(\frac{1}{2}m_w+m_r)\sin\theta_0}{m_r l A(\theta_0)} & 0 \\ 0 & 0 & 0 & 0 & 0 \\ 0 & 0 & 0 & 0 & K_3 \\ 0 & 0 & 0 & 0 & 0 \end{bmatrix}; \tag{9}$$

$$\mathbf{C} = \begin{bmatrix} 1 & 0 & 0 & 0 & 0 & 0 \\ 0 & 0 & 1 & 0 & 0 & 0 \\ 0 & 0 & 0 & 1 & 0 & 0 \\ 0 & 0 & 0 & 0 & 1 & 0 \end{bmatrix}; \tag{10}$$

$$\mathbf{D} = \begin{bmatrix} 0 & 0 & 0 & 0 & 0 \\ 0 & 0 & 0 & 0 & 0 \\ 0 & 0 & 0 & 0 & 0 \\ 0 & 0 & 0 & 0 & 0 \end{bmatrix}; \tag{11}$$

$$A(\theta) = \tfrac{1}{2}m_w + m_r\sin^2\theta; \tag{12}$$

$$B(\theta) = \tfrac{1}{2}m_w + m_r(1+\cos^2\theta); \tag{13}$$

$$\begin{aligned} K_1 = & -2m_r F_{m0}\cos\theta_0\sin\theta_0 \\ & + 2m_r\tfrac{b}{r_w^2}v_0\cos\theta_0\sin\theta_0 \\ & + F_{z0}\left(B(\theta_0)\sin^2\theta_0 - A(\theta_0)\cos^2\theta_0\right) \\ & + m_r g\left(B(\theta_0)\sin\theta_0\sin(\theta_0+\alpha_0)\right) \\ & - m_r g\left(A(\theta_0)\cos\theta_0\cos(\theta_0+\alpha_0)\right) \\ & + m_w F_{x0}\cos\theta_0\sin\theta_0 \\ & + m_r l\omega_0^2\cos\theta_0(2m_r\sin^2\theta_0 - A(\theta_0)) \\ & - 2m_r(m_w+m_r)g\sin\alpha_0\cos\theta_0\sin\theta_0; \end{aligned} \tag{14}$$

$$\begin{aligned} K_2 = & -(\tfrac{1}{2}m_w + m_r)F_{z0}\cos\theta_0(2m_r\sin^2\theta_0 - A(\theta_0)) \\ & - 2(\tfrac{1}{2}m_w + m_r)m_r^2 g\cos\theta_0\sin\theta_0\sin(\alpha_0+\theta_0) \\ & - (\tfrac{1}{2}m_w + m_r)m_r g A(\theta_0)\cos(\alpha_0+\theta_0) \\ & - \tfrac{1}{2}m_w F_{x0}\sin\theta_0 B(\theta_0) + m_r F_{m0}\sin\theta_0 B(\theta_0) \\ & + m_r(m_w+m_r)g\sin\alpha_0 B(\theta_0)\sin\theta_0 \\ & - m_r\tfrac{b}{r_w^2}v_0\sin\theta_0 B(\theta_0) \\ & + m_r^2 l\omega_0^2(B(\theta_0)\sin^2\theta_0 - A(\theta_0)\cos^2\theta_0); \end{aligned} \tag{15}$$

$$K_3 = \frac{12\cos\theta_0}{m_r(l_p^2\sin^2\theta_0 + d_p^2\cos^2\theta_0 + w_p^2)}; \tag{16}$$

$$K_4 = -\frac{\begin{pmatrix}12\tau_0\sin\theta_0(l_p^2\sin^2\theta_0 \\ +(2l_p^2 - d_p^2)\cos^2\theta_0 + w_p^2)\end{pmatrix}}{m_r(l_p^2\sin^2\theta_0 + d_p^2\cos^2\theta_0 + w_p^2)^2}; \tag{17}$$

$$K_5 = \frac{\begin{pmatrix}-m_r g\cos\theta_0\cos(\alpha_0+\theta_0) \\ +(m_w+m_r)g\cos\alpha_0\end{pmatrix}}{A(\theta_0)}; \tag{18}$$

$$K_6 = \frac{\begin{pmatrix}(\frac{1}{2}m_w+m_r)m_r g\cos(\alpha_0+\theta_0) \\ -m_r(m_w+m_r)g\cos\alpha_0\cos\theta_0\end{pmatrix}}{m_r l A(\theta_0)}. \tag{19}$$

The set of models given by (4) and (5) is unsuited for control purposes, as it is uncontrollable when $\theta_0 = 0$. This can be resolved by dismissing unnecessary system outputs. Considering that $\Delta\phi$ and $\Delta\dot{\phi}$ cannot be controlled by the motor, their control being fully dependent on the user, and that the other outputs are not reliant on them, they can be discarded without altering the controller output. Similarly, the inclusion of Δx is entirely redundant, as its first derivative Δv is already included in the model. Their removal leads to the set of models defined by

$$\dot{\mathbf{x}}' = \mathbf{A}'\mathbf{x}' + \mathbf{B}'\mathbf{u}', \tag{20}$$

$$\mathbf{y}' = \mathbf{C}'\mathbf{x}' + \mathbf{D}'\mathbf{u}', \tag{21}$$

where

$$\mathbf{x}' = \begin{bmatrix}\Delta v & \Delta\omega & \Delta\theta\end{bmatrix}^T; \tag{22}$$

$$\mathbf{u}' = \begin{bmatrix}\Delta\alpha & \Delta F_m & \Delta F_x & \Delta F_z\end{bmatrix}^T; \tag{23}$$

$$\mathbf{A}' = \begin{bmatrix} -\dfrac{b}{r_w^2 A(\theta_0)} & \dfrac{2m_r l\omega_0 \sin\theta_0}{A(\theta_0)} & \dfrac{K_1}{A(\theta_0)^2} \\ \dfrac{m_r b \cos\theta_0}{m_r l r_w^2 A(\theta_0)} & -\dfrac{2m_r^2 l\omega_0 \sin\theta_0 \cos\theta_0}{m_r l A(\theta_0)} & \dfrac{K_2}{m_r l A(\theta_0)^2} \\ 0 & 1 & 0 \end{bmatrix}; \quad (24)$$

$$\mathbf{B}' = \begin{bmatrix} K_5 & \dfrac{1}{A(\theta_0)} & \dfrac{1-\cos^2\theta_0}{A(\theta_0)} & \dfrac{-\cos\theta_0 \sin\theta_0}{A(\theta_0)} \\ K_6 & \dfrac{-m_r \cos\theta_0}{m_r l A(\theta_0)} & \dfrac{\frac{1}{2} m_w \cos\theta_0}{m_r l A(\theta_0)} & \dfrac{(\frac{1}{2} m_w + m_r)\sin\theta_0}{m_r l A(\theta_0)} \\ 0 & 0 & 0 & 0 \end{bmatrix}; \quad (25)$$

$$\mathbf{C}' = \begin{bmatrix} 1 & 0 & 0 \\ 0 & 1 & 0 \\ 0 & 0 & 1 \end{bmatrix}; \quad (26)$$

$$\mathbf{D}' = \begin{bmatrix} 0 & 0 & 0 & 0 \\ 0 & 0 & 0 & 0 \\ 0 & 0 & 0 & 0 \end{bmatrix}. \quad (27)$$

Unlike the previous models, these models are controllable at $\theta_0 = 0$, and thus can be used with the controller detailed in the forthcoming section.

4. Controller

The controller for the cane is based on a linear-quadratic regulator (LQR). The gain matrix K is calculated by minimizing the LQR cost function,

$$J = \int_0^\infty (x^T Q x + u^T R u)\, dx. \quad (28)$$

The input weight matrix Q was set empirically to values in which all the output variables stabilized in a relatively short amount of time. In this case, an acceptable matrix Q was found to be

$$Q = \begin{bmatrix} 100 & 0 & 0 \\ 0 & 10 & 0 \\ 0 & 0 & 100 \end{bmatrix}. \quad (29)$$

The output weight matrix R was set as the identity matrix of size $n = 5$.

Gain-scheduling is an adaptive control method that consists of linearizing the problem around multiple operating points and, at each moment of operation, using the linearized model that best fits the current operating parameters. This method was selected for its simplicity relative to other adaptive control methods, considering the objective of implementing the control system on a microcontroller embedded in the cane.

In this case, the implementation of gain-scheduling manifests as the addition of a gain-scheduler block a basic LQR. This block updates the operating point of the system and calculates the new matrices $\mathbf{A}'$, $\mathbf{B}'$, $\mathbf{C}'$ and $\mathbf{D}'$ of the linearized state-space model. The latter function is attained by plugging the current operating point variables into the matrices in equations (4) and (5). The first two matrices are then fed to the LQR block, which computes the LQR gain for the current linearized model. The complete schematic of the controller is illustrated in figure 3.

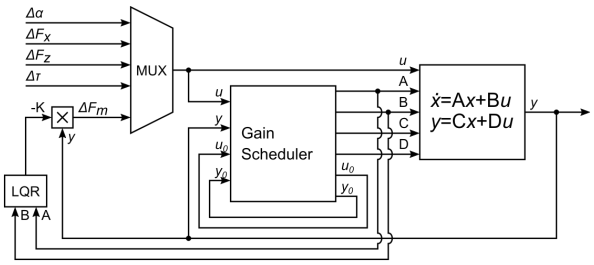

Figure 3: Gain-scheduled LQR feedback controller.

4.1. Simulations

The gain-scheduled LQR controller was simulated using *Simulink*. In the first simulation, the adaptability of the cane to the user's walking speed was assessed by varying the horizontal force (F_x) applied by the user to the handle. Specifically, F_x is gradually increased from 0 N to 10 N after $t = 5$ s and then to 20 N after $t = 15$ s. The results, shown in figure 4, confirm the adaptability of the control system to user characteristics. By applying horizontal force to the handle, the user can effectively change the velocity and angle of the cane. Moreover, in periods when the force applied to the handle is constant, the cane exhibits a stable behaviour. However, there are some small oscillations in the initial stages of the simulation, before the controller finds the initial equilibrium position.

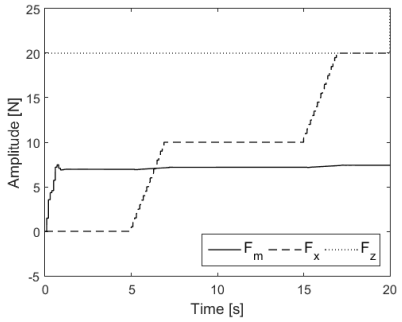

(a) F_m (solid line), F_x (dashed line) and F_z (dotted line).

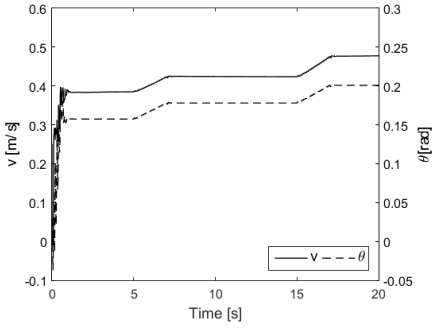

(b) v (solid line) and θ (dashed line).

Figure 4: Simulation of the model with varying F_x.

In the second simulation, the robustness of the system in situations of sudden loss of equilibrium was assessed by applying a downward force of 100 N at $t = 10$ s, simulating the user transferring their body weight to the cane. As can be seen in figure 5, the control system successfully returns to an equilibrium after significant downward pressure is applied to the handle, without critical deviations from the initial operating point. Notwithstanding, both the angle and velocity exhibit undesired, albeit expected, fluctuations immediately after the change.

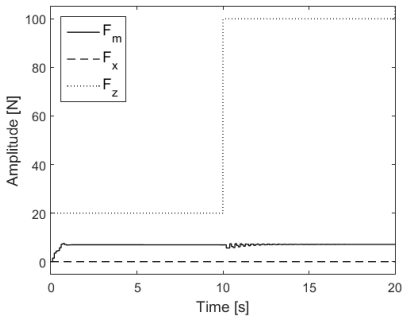

(a) F_m (solid line), F_x (dashed line) and F_z (dotted line).

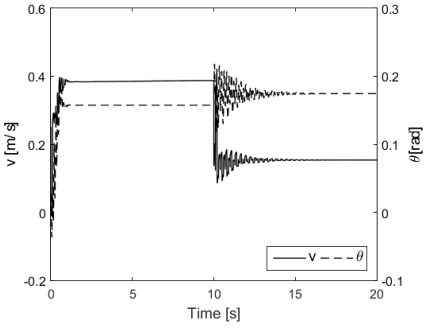

(b) v (solid line) and θ (dashed line).

Figure 5: Simulation of the model with a sudden variation F_z.

Both simulations were repeated with $0.01\,\mathrm{W\,Hz^{-1}}$ white noise added to F_x and F_z, $10^{-5}\,\mathrm{W\,Hz^{-1}}$ white noise added to the measurements of v and ω and $10^{-6}\,\mathrm{W\,Hz^{-1}}$ white noise added to the measurement of θ. The results from the first simulation with added white noise are presented in figure 6. These results demonstrate the system's effectiveness in dealing with noise. Although the relation between the input and the output becomes less clear, there is still a perceptible upward trend in the velocity and angle as the horizontal force is increased.

The results from the second simulation with added white noise are presented in figure 7. These results again confirm the system's ability to deal with noise, given the prompt reaction to the change in F_z, arguably better when compared to the experiment without added white noise, as the oscillations are attenuated more rapidly.

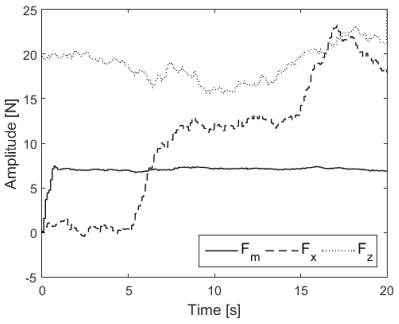

(a) F_m (solid line), F_x (dashed line) and F_z (dotted line).

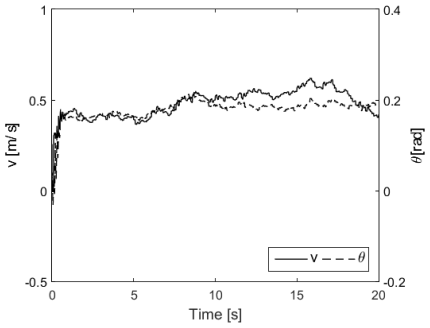

(b) v (solid line) and θ (dashed line).

Figure 6: Simulation of the model with varying F_x and added white noise.

4.2. Physical Implementation

The cane is actuated by a motor controlled by an Arduino UNO WiFi REV2 microcontroller. The angle of the cane θ is measured with an inertial measurement unit, the distance x is measured with an encoder, and the user-applied forces are measured using an force sensing resistor (FSR) installed in the cane handle. While the theoretical model assumes the independence of F_x and F_z, only one FSR is used for control purposes, meaning that F_x and F_z are calculated as the horizontal and vertical components of the measured force. There is an additional FSR that serves as a backup, however the two sensors cannot be used to independently measure the different components of the force since they are mounted with the same orientation.

Given the infeasibility of on-board LQR gain calculation due to unacceptably high latency, LQR gain matrices were pre-calculated using *MATLAB* and saved to a lookup table (LUT). At each loop iteration, the Arduino consults the LUT in order to select the matrix that best fits the current operating point variables. There are 7 variables on which the operating point depends: v_0, ω_0, θ_0, α_0, F_{m0},

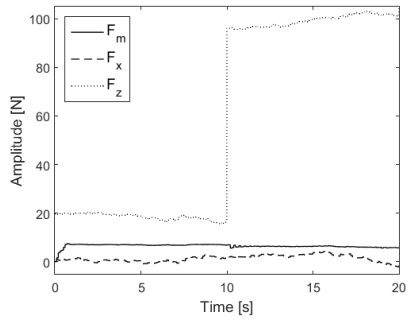

(a) F_m (solid line), F_x (dashed line) and F_z (dotted line).

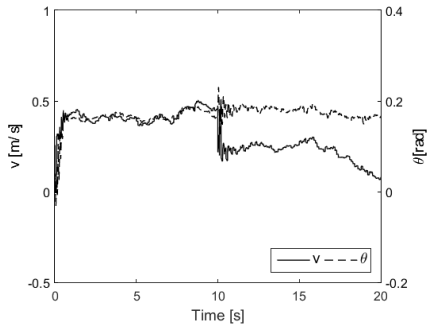

(b) v (solid line) and θ (dashed line).

Figure 7: Simulation of the model with a sudden variation F_z and added white noise.

F_{x0} and F_{z0} (τ_0 has no influence on the control). Therefore, the LUT consists of n^7 matrices, where n is the number of steps for each variable. The specific Arduino used has 6144 B of variable storage space, which is manifestly insufficient for any useful LUT. Thus, an SD card reader was added to allow for external storage.

A 6-step LUT was implemented, as it provides a good balance between latency and accuracy. The steps used are listed in table 3.

Table 3: Variable steps used in 6-step LQR gain computation.

Variable	Steps					
v_0 [m s^{-1}]	-1	-0.6	-0.2	0.2	0.6	1
ω_0 [rad s^{-1}]	-2	-1.2	-0.4	0.4	1.2	2
θ_0 [rad]	-0.785	-0.471	-0.157	0.157	0.471	0.785
α_0 [rad]	-0.785	-0.471	-0.157	0.157	0.471	0.785
F_{m0} [N]	-20	-12	-4	4	12	20
F_{x0} [N]	-100	-60	-20	20	60	100
F_{z0} [N]	-100	-60	-20	20	60	100

5. Results

This section describes the real-world tests that were performed in order to assess the viability of the concept and analyses their results.

5.1. Specific Tests

A series of simple tests were devised to assess the real-world effectiveness of each desired functionality of the control system. The following tests were all performed by a healthy individual without any motor difficulties and prior cane usage, but with familiarity with the controlled cane.

Test 1 consists of the user walking at a constant pace while keeping the cane nearly vertical. This test aims to assess the stability of the control system, as well as to allow for an estimation of real-world noise introduced by the user. The outcome of this test is depicted in figure 8, showing that the user was able to keep a steady velocity and a somewhat steady angle while using the cane.

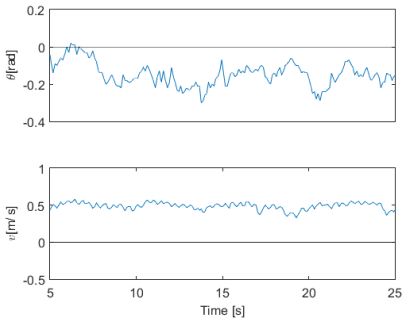

Figure 8: Results of test 1.

Test 2 consists of the user simulating a situation of imbalance by applying downward and forward pressure to the handle. This test aims to assess the forward fall prevention capabilities of the control system. Figure 9 depicts the results of this test, confirming that the controller reacts effectively to imbalance by halting cane movement. The cane is able to support the weight of the user and regains equilibrium after the disturbance.

Test 3 consists of the user simulating a situation of imbalance by applying downward and backward pressure to the handle. This test aims to assess the back fall prevention capabilities of the control system. Once again, the results confirm that the controller reacts effectively to imbalance by halting cane movement, as depicted in figure 10. Nevertheless, it should be noted that the manner in which the latter two tests were conducted may not reflect the manner in which actual real-world falls occur, meaning that further research is necessary to accurately assess the fall prevention capabilities of the controlled cane.

Test 4 consists of the user walking with the cane at an increasing pace. This test aims to assess the adaptability of the control system to the walking pace of the user. Figure 11 displays the results from this test, which show that the user is able to gradually increase and decrease the cane speed at will.

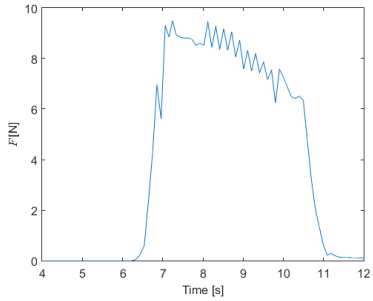

(a) Total force applied by the user.

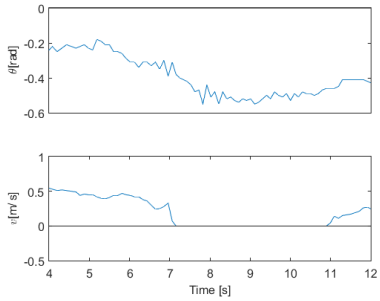

(b) θ and v.

Figure 9: Results of test 2.

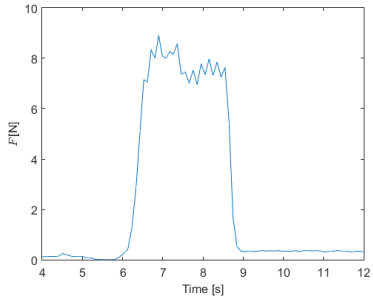

(a) Total force applied by the user.

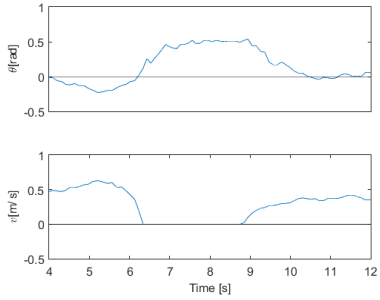

(b) θ and v.

Figure 10: Results of test 3.

Test 5 consists of the user walking with the cane at an angle. This test aims to assess the adaptability of the control system to the preferred cane angle of the user. Figure 12 depicts the results from this test, which show that the user is able to increase the cane angle and walk stably with a cane angle of around -0.4 rad.

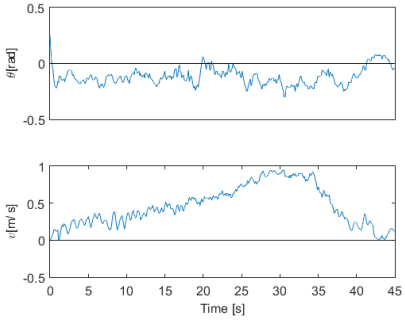

Figure 11: Results of test 4.

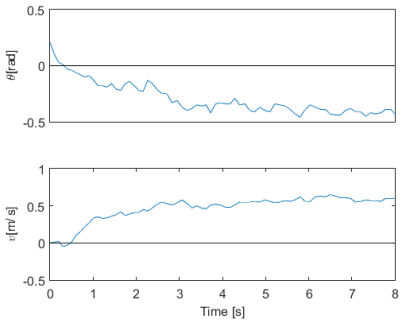

Figure 12: Results of test 5.

Test 6 entails the repetition of test 5 in an uneven surface. This test aim to assess the resilience of the control system when subject to additional noise. Figure 13 displays the results from this test, showing that the control system does not behave as well when using the cane on an uneven surface. Since the unevenness of the terrain adds noise to the measurement of the angle θ, it frequently surpasses the threshold for fall detection, causing the controller to undesirably stop cane movement.

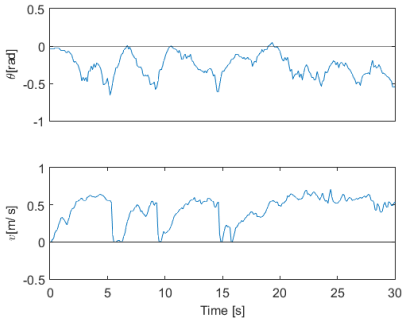

Figure 13: Results of test 6.

Finally, test 7 consists of the user keeping the cane in a still position. Figure 14 depicts the results from this test, which show that the controller at times induces unprompted movement, however

the user is able to keep movement to a minimum without significant effort.

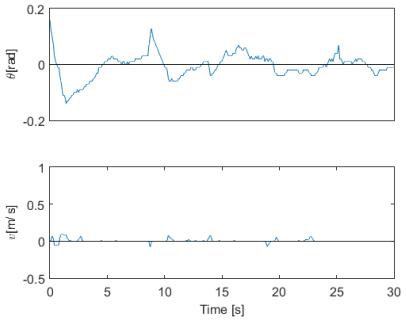

Figure 14: Results of test 7.

5.2. Generic Tests

Aside from the preceding feature-specific tests, more generic walking tests were devised, so as to appraise the intuitiveness and effectiveness of the control system, as well as to gauge the sense of safety felt by the users when using the controlled cane. These tests were administered to elderly individuals with varying degrees of mobility impairments, with some having had prior experience with regular walking canes. Although the obtained results vary significantly depending on the user, the learning curve for the usage of the cane generally proved shallow, especially among people with no previous cane usage experience, and the cane generally exhibited a smooth behaviour in normal operating conditions. Moreover, it was observed that users tended to keep the cane in front of them at an angle ($\theta < 0$), predominantly around $-0.4\,\text{rad}$, confirming the findings by Neves et al. [8]. However, the mechanism implemented to avoid falls proved to be too sensitive for some people's usage characteristics, stopping the cane when the user applied regular force to the handle.

Figure 15 depicts an example of a typical user with lesser support needs, showing the relatively small force applied by the user to the handle. Accordingly, the cane maintains forward movement, without unwanted stops and with few large velocity variations. Note that the negative peak around $t = 70\,\text{s}$ is an outlier likely caused by a numeric artifact in the calculation of v.

Contrarily, figure 16 depicts an example of a user with greater support needs, manifesting a significantly higher force applied to the cane handle. As a consequence, the user-applied force frequently surpasses the force threshold set to avoid falls, halting the cane mid-movement.

5.3. Comparison with Controller by Neves et al.

The control approach developed in this thesis was compared against the control approach developed

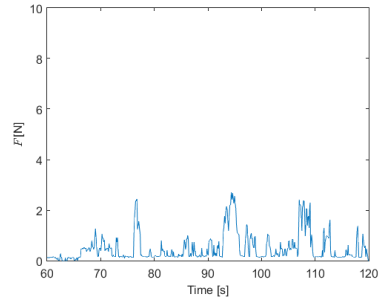

(a) Total force applied by the user.

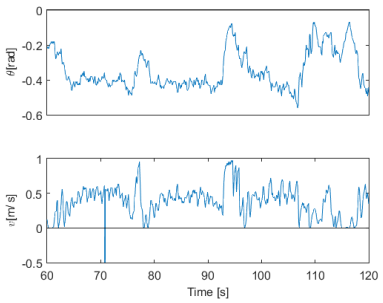

(b) θ and v.

Figure 15: Example of user with lesser support needs.

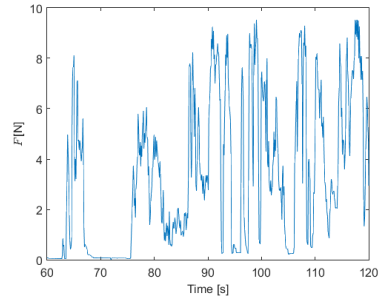

(a) Total force applied by the user.

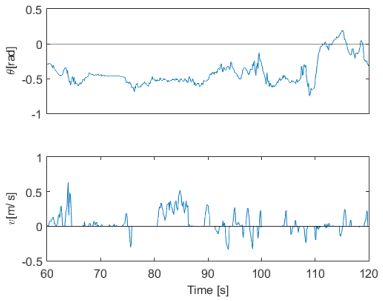

(b) θ and v.

Figure 16: Example of user with greater support needs.

by Neves et al. [8] for an identical prototype, in order to assess the potential advantages and disadvantages of each. The controller consists of an LQR that takes into account the user's force input,

aiming to provide a similar movement to that of a regular cane by accompanying the movement of the opposite leg, although without the need to lift the cane off the ground [7].

The results from the comparison with the second control approach once again reveal a significant difference between users, although it is possible to observe some trends. For instance, most users analysed apply more force when using the cane with the gain-scheduled LQR control, as in figure 17, even though a few users applied more force with the LQR with force input, as in figure 18. This may be related to the adaptability of users to each control system, as it was found that most people, especially those without prior cane usage, tended to adapt faster to the gain-scheduled control.

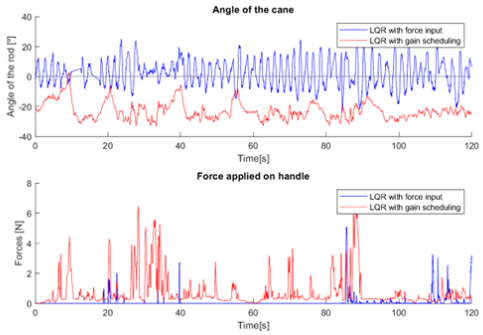

Figure 17: Example of user applying more force with gain-scheduled control.

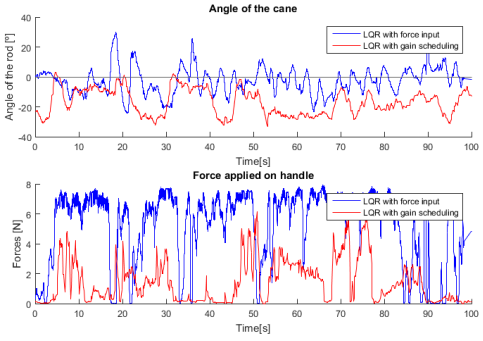

Figure 18: Example of user applying more force with LQR with force input.

What is common across all users is the tendency to use the cane with the gain-scheduled LQR control at a negative angle θ, that is, keep the cane in front of them, while oscillating the cane with the LQR with force input between positive and negative angles. This is expected behaviour, since in the former case the controller is designed to keep the angle relatively stable while in the latter case the controller is designed to accompany the movement of the opposite leg. It should be noted, however, that the peaks in user-applied force in the gain-scheduled control incorrectly trigger the fall detection mechanism, causing the angle to approach 0°.

All in all, the controller developed in this thesis compared favorably against the controller by Neves et al. [8] when it comes to intuitiveness, especially for users without prior cane usage experience. However, it transmits less of a sense of security, particularly for regular users of traditional canes.

5.4. Gini Coefficient Comparison

In order to further understand the differences between the control approaches, the Gini coefficient was applied to the cane angle and the control signal. The Gini coefficient provides a measure of sparsity within a data set, with multiple studies finding it the most adequate sparsity indicator [4, 9]. In this application, the concept of sparsity is particularly useful as it indicates whether the cane angle and the control signal are mostly concentrated around a specific value (Gini coefficient closer to 0) or are spread somewhat evenly (Gini coefficient closer to 1). As such, lower Gini coefficients are preferable.

Table 5.4 displays the Gini coefficients for each test conducted in the last subsection (tests 1-7) and for two additional tests performed by individuals without mobility impairments (tests 8 and 9) [7].

Table 4: Gini coefficients.

	Cane angle		Control signal	
Test	LQR w/ force input	LQR w/ gain scheduling	LQR w/ force input	LQR w/ gain scheduling
1	0.50904	0.29836	0.48201	0.24211
2	0.38884	0.27097	0.38799	0.44213
3	0.44663	0.18598	0.41844	0.13918
4	0.41002	0.2349	0.48174	0.49297
5	0.41046	0.36213	0.36169	0.26449
6	0.36914	0.32826	0.38826	0.40967
7	0.37402	0.32433	0.43674	0.5396
8	0.39373	0.28707	0.49549	0.12486
9	0.32376	0.35676	0.45030	0.20661

Apart from the last test, all Gini coefficients of cane angles are lower for the gain-scheduled controller developed in this thesis than for Neves et al.'s second controller. This should be expected, given that the latter controller encourages the user to vary the angle while walking, leading to a wider range of cane angles. Nonetheless, these results show that the gain-scheduled controller is effective at keeping the cane angle relatively stable. When it comes to the control signal, however, the Gini coefficients for the gain-scheduled controller exhibit more inconsistency, with some Gini values being comparable or greater than those for Neves et al.'s second controller. This might be caused by erroneous fall de-

tections, which are more prominent in users with greater support needs, and thus cause more variability in the control signal.

6. Conclusions

The sustained growth in the World's elderly population has prompted an increase in demand for walking aids. While robotic improvements to walkers have been thoroughly studied and developed by several academics, lesser attention has been dedicated to the robotic enhancement of standard walking canes. The control system proposed in this thesis aims to address some of the shortcomings of walking canes, including the relative lack of stability and ease of use, and thus ameliorate the quality of life of people with reduced mobility. To that end, a gain-scheduled LQR controller was devised.

The viability of the control approach described in this thesis is suggested by the test results. The control system satisfactorily fulfilled the objectives delineated previously, displaying smooth and intuitive behaviour in normal standing and walking conditions. The system was also responsive in situations of potential imbalance, thereby potentially mitigating accidents, and demonstrated a resilience to typical noise conditions. Moreover, the system proved adaptable to user walking characteristics, namely the cane angle and walking speed.

However, some deficiencies in the developed controller were identified. Firstly, while the controller is indeed responsive to certain situations of inbalance, these were not studied in depth in this thesis, meaning that the controller may struggle to react in other unenumerated situations. Additionally, the mechanisms to prevent inbalance have in some cases proven to be too sensitive, halting motor movement during regular walking.

As future work, improved fall prevention mechanisms will be studied in order to further reduce accidents and transmit a better sense of security to the cane users. Furthermore, alternative adaptive control techniques, including machine learning algorithms, will be investigated and compared with the gain-scheduling controller developed in this thesis. The tests that were performed indicate that users reveal considerable differences in walking patterns and support needs that were not contemplated in this control method; machine learning can potentially further adjust the control to each user.

Acknowledgements

Firstly, I would like to express my deep gratitude to my thesis supervisor, Professor João Silva Sequeira, for the crucial advice provided throughout the course of this thesis. I would also like to extend my gratitude to Gonçalo Neves, who contributed greatly to this thesis by providing the hardware prototype and helping set up the real-world tests.

Finally, I would also like to thank my parents for expending their time to help test the cane and for the invaluable feedback they provided.

References

[1] World population prospects 2019: Volume II: Demographic profiles. United Nations, Department of Economic and Social Affairs, Population Division, 2019. Accessed 2021-11-23.

[2] R. Ady, W. Bachta, and P. Bidaud. Development and control of a one-wheel telescopic active cane. In *5th IEEE RAS/EMBS International Conference on Biomedical Robotics and Biomechatronics*, pages 461–466. IEEE, 2014.

[3] J. A. Harvey, S. F. Chastin, and D. A. Skelton. How sedentary are older people? A systematic review of the amount of sedentary behavior. *Journal of aging and physical activity*, 23(3):471–487, 2015.

[4] N. Hurley and S. Rickard. Comparing measures of sparsity. *IEEE Transactions on Information Theory*, 55(10):4723–4741, 2009.

[5] M. M. Martins, C. P. Santos, A. Frizera-Neto, and R. Ceres. Assistive mobility devices focusing on smart walkers: Classification and review. *Robotics and Autonomous Systems*, 60(4):548–562, 2012.

[6] H. B. Menz, S. R. Lord, and R. C. Fitzpatrick. Age-related differences in walking stability. *Age and ageing*, 32(2):137–142, 2003.

[7] G. Neves, J. S. Sequeira, and P. Bollinger. Behavioral variations of a robotic cane in distinct control situations, 2022. Manuscript submitted for publication.

[8] G. Neves, J. S. Sequeira, and C. Santos. Lightweight locomotion assistant for people with mild disabilities. In *Climbing and Walking Robots Conference*, pages 465–476. Springer, 2021.

[9] Y. Parkale and S. Nalbalwar. Investigation on 1-D and 2-D signal sparsity using the Gini index, L1-norm and L2-norm for the best sparsity basis selection. In *International Conference on Communication and Signal Processing 2016 (ICCASP 2016)*, pages 630–639. Atlantis Press, 2016.

[10] P. Van Lam and Y. Fujimoto. Completed hardware design and controller of the robotic cane using the inverted pendulum for walking assistance. In *2017 IEEE 26th International Symposium on Industrial Electronics (ISIE)*, pages 1935–1940. IEEE, 2017.